Ceramics-Silikáty 66 (2), 188-201 (2022)
www.ceramics-silikaty.cz doi: 10.13168/cs.2022.0013

UNIAXIAL COMPRESSIVE STRESS-STRAIN BEHAVIOUR OF RECYCLED AGGREGATE CONCRETE PREPARED WITH CARBONATED RECYCLED CONCRETE AGGREGATES

JUN WU*, #YAHONG DING*, PING XU*, MEIXIANG ZHANG*, **, MENG GUO*, SHUQI GUO*

*School of Civil Engineering, Henan Polytechnic University, Jiaozuo 454003, China
**School of Architectural Engineering, Xinyu University, Xinyu 338004, China

#E-mail: dingyahong@hpu.edu.cn

Submitted January 18, 2022; accepted February 28, 2022

Keywords: Stress-strain curve, Constitutive model, Recycled concrete aggregate, Limewater, Accelerated carbonation, Interfacial transition zone

The influences of carbonated recycled concrete aggregate (CRCA) on the stress-strain behaviour of recycled aggregate concrete (RAC) were studied. Recycled concrete aggregate (RCA) pre-soaked in limewater was processed by accelerated carbonation for 24 h, whose pressure was 0.30 MPa. Four substitution ratios (0 %, 30 %, 70 %, 100 %) of the aggregate were utilised. RMT-150C rock mechanics test system (frame stiffness of 5 MN/mm, loading rate of 0.005 mm·s^{-1}) was used to conduct the tests. The results showed that the failure modes of all specimens were shear failure, but the failure angles of RAC and CRAC (RAC prepared with CRCA) were larger than those of natural aggregate concrete (NAC), which were in the range of 63° – 75° and 58° – 64° respectively. As the substitution ratio of RCA increasing, the stress-strain curve of RAC gradually flattened, which meant its brittleness decreased. Moreover, its peak stress, elastic modulus, and peak strain decreased continuously, while its ultimate strain increased continuously. Compared with RAC, CRAC showed the similar stress-strain curve, but its brittleness was slightly higher. Furthermore, its peak stress, elastic modulus, and peak strain increased, while its ultimate strain decreased. Finally, based on linear regression analysis and relevant standards, the prediction models of peak stress, elastic modulus, peak strain, and ultimate strain, as well as the stress-strain constitutive models of RAC and CRAC were proposed, which had a good applicability to the test data. In conclusion, the stress-strain behaviour of CRAC were similar to that of RAC.

INTRODUCTION

With the rapid development of economy, a large number of old buildings in the cities are being demolished every year, and the construction and demolition waste (C&DW) piled in the suburbs poses a serious threat to the ecological environment [1]. At the same time, the construction of new buildings needs to consume massive concrete, but the finite natural aggregate (NA) resources are difficult to meet this demand. Hence, for the purpose of solving the problems of environmental pollution caused by C&DW and the lack of NA resources, RCA obtained from C&DW can be recycled to replace NA [2].

Nevertheless, the quality of RCA is worse than that of NA because of the attached old mortar (OM), which makes its apparent density lower, its water absorption and crushing value higher [3]. Furthermore, RAC has three types of interfacial transition zone (ITZ), namely ITZ-1 between NA and new mortar (NM), ITZ-2 between NA and OM, ITZ-3 between OM and NM, while NAC only has ITZ-1 [4]. As a result, RAC are worse than NAC in terms of mechanical property and durability, because ITZ has the poorest property [5]. Hence, for promoting the application of RAC, the quality of RCA should be improved firstly. At present, accelerated carbonation can not only improve the quality of RCA [6], but also can alleviate the greenhouse effect by absorbing CO_2, therefore it has great application prospects in engineering field.

In addition, the stress-strain behaviour is an important basis for the design of concrete structures. The research found that as the substitution ratio of RCA increasing, the stress-strain curve of RAC is similar to that of NAC, but its peak stress and elastic modulus increase [7], while its peak strain and ultimate strain decrease [8, 9]. However, the quality of CRCA is improved by accelerated carbonation, which has a certain impact on the stress-strain behaviour of CRAC. For example, Li [10] studied the influences of strain rate on the uniaxial dynamic compressive behaviour of RAC, and found that the peak stress and elastic modulus of CRAC are higher than those of RAC, but their strain rate sensitivities are less obvious than those of RAC. Moreover, Luo [11] found that compared with RAC, as the properties of ITZ-3 in CRAC are improved, the slope of ascending branch and peak stress in the stress-strain curve increase, while the peak strain decreases.

The research found that the quality of RCA can be further improved by accelerated carbonation provided

that the extra calcium ions are introduced [12], because calcite promotes calcium silicate hydrate to nucleate and grow [13], and monocarbonate can also be generated in ITZ-3 by the reaction between calcite and aluminate, thus improving the properties of ITZ-3 [14]. Besides, the properties of ITZ have an important impact on the mechanical properties and stress-strain behaviour of RAC [15]. However, the influences of CRCA, which is obtained by introducing calcium ions into RCA and then treating it by accelerated carbonation, on the stress-strain behaviour of CRAC still lack research.

Therefore, to study the influences of CRCA on the stress-strain behaviour of CRAC, RCA pre-soaked in limewater was processed by accelerated carbonation for 24 h, whose pressure was 0.30 MPa. Based on linear regression analysis and relevant standards, the prediction models of peak stress, elastic modulus, peak strain, and ultimate strain, as well as the stress-strain constitutive models of RAC and CRAC were proposed.

EXPERIMENTAL

Materials

Cementitious materials

The P•O 42.5 ordinary Portland cement (specific surface area of 3550 $cm^2 \cdot g^{-1}$, density of 3.14 $g \cdot cm^{-3}$) was utilised, with its constituents showed in Table 1.

Fine aggregate

Based on standard GB/T 14684-2011, the indexes of the natural river sand are showed in Table 2. Besides, its passing percentages are showed in Figure 1, with a fineness modulus of 2.84.

Coarse aggregate

RCA was obtained by crushing C30 reinforced concrete members which were six-month old. Based on standard GB/T 14685-2011, the indexes of NA and RCA are showed in Table 2, and their passing percentages

Table 1. The constituents in cement.

Constituents	CaO	SiO_2	Al_2O_3	Fe_2O_3	MgO	K_2O	Na_2O	SO_3	LOI
Percentage (%)	65.67	22.35	5.42	3.56	1.54	0.46	0.68	0.65	2.53

Table 2. The indexes of the aggregate.

Aggregate	Grain diameter (mm)	Crushing value (%)	Water absorption (%)	Apparent density ($kg \cdot m^{-3}$)
Sand	0-4.75	25.35	0.70	2629
NA-1	5-10	13.41	0.55	2703
NA-2	10-20	11.11	0.60	2723
RCA-1	5-10	23.87	5.85	2690
RCA-2	10-20	16.11	3.74	2697
CRCA-1	5-10	22.81	4.74	2697
CRCA-2	10-20	14.93	3.34	2707

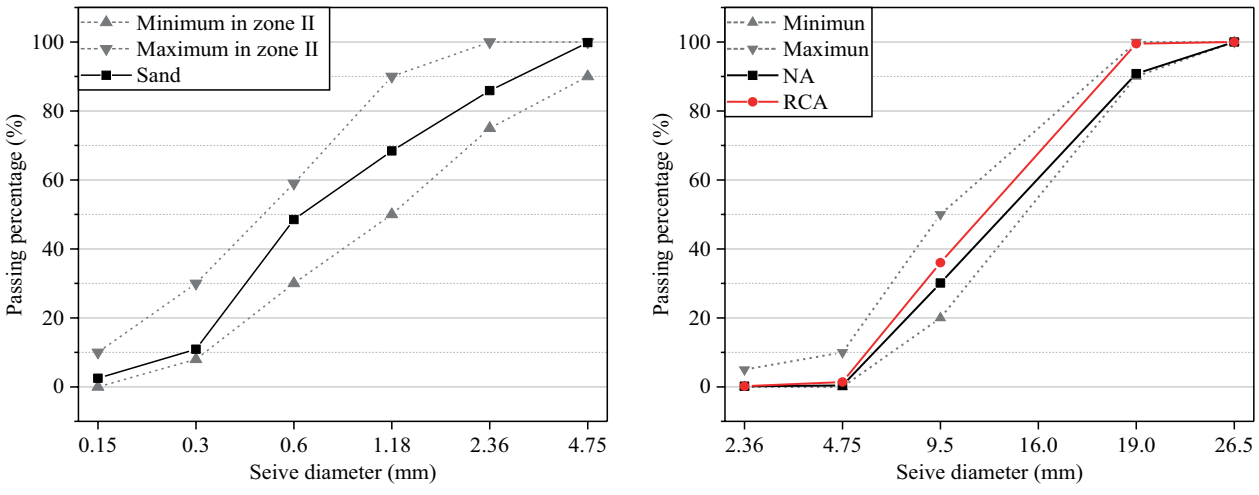

a) fine aggregate b) coarse aggregate

Figure 1. The passing percentages of aggregate: a) fine aggregate; b) coarse aggregate.

are showed in Figure 1, whose mass ratio was 0.50 for 5-10 mm and 10-20 mm.

Accelerated carbonation

The accelerated carbonation equipment (volume of 50 L) is showed in Figure 2, and CO_2 with purity exceeding 99 % was utilised. Firstly, RCA was pre-soaked in limewater and then processed in a constant temperature and humidity box (temperature 20 °C, humidity 70 %) for 24 h, respectively. Before accelerated carbonation, the pressure in the equipment was processed to -0.06 MPa using a vacuum pump. During accelerated carbonation, the pressure was remained at 0.30 MPa and lasted for 24 h. Finally, based on standard GB/T 14685-2011, the indexes of CRCA are showed in Table 2.

Figure 2. Accelerated carbonation equipment.

Mix proportions

Based on standards JGJ 55-2011 and JGJ/T 443-2018, the mix proportions of RAC (C40, water-cement ratio of 0.49) were designed, as showed in Table 3. The coarse aggregate in saturated surface dry state was used in mixing process, with mass ratio of 0.50 for 5-10 mm and 10-20 mm.

Specimen preparation

The specimens of RAC were prepared and cured based on standard GB/T 50081-2019. The cubic specimens with size of 100 × 100 × 100 mm were tested for compressive strength, while prismatic specimens with size of 100 × 100 × 300 mm were tested for stress-strain behaviour. All the specimens were prepared by the forced concrete mixer and vibration table and then cured in the standard curing box (temperature 20 °C, humidity 95 %) for 28 days.

Test methods

Based on standard GB/T 50081-2019, as showed in Figure 3, RMT-150C rock mechanics test system (frame stiffness of 5 MN/mm) was used to conduct the tests, with the loading rates of 0.005 mm/s and 0.5 MPa·s^{-1} for the stress-strain behaviour and compressive strength.

Based on Saint-Venant's principle, the uneven vertical compressive stresses and the horizontal friction forces with zero resultant force on the loading end faces of the specimen, have significant impacts on the stress state of the specimen in the range of height approximately equalling to the width of the specimen section. Therefore, in order to obtain more accurate uniaxial compressive stress-strain behaviour, two displacement meters were symmetrically installed in the middle of the specimen on both sides, thus the displacement in the range of 100 mm could be obtained. The displacement test device is showed in Figure 4. Before the formal test, the specimen was preloaded for three times to align the specimen and ensure the displacement meters working normally, with the preload about 0.3 times of the ultimate load. During the test, the data of load and displacement were collected synchronously by RMT-150C rock mechanics test system.

Table 3. The mix proportions of RAC.

Specimen number	Substitution ratio (%)	Cement (kg·m^{-3})	Sand (kg·m^{-3})	Water (kg·m^{-3})	NA (kg·m^{-3})	RCA (kg·m^{-3})	CRCA (kg·m^{-3})	Slump (mm)
NAC	0	440	611	215	1134	0	0	105
RAC-1	30	440	611	215	794	340	0	100
CRAC-1	30	440	611	215	794	0	340	100
RAC-2	70	440	611	215	340	794	0	95
CRAC-2	70	440	611	215	340	0	794	90
RAC-3	100	440	611	215	0	1134	0	90
CRAC-3	100	440	611	215	0	0	1134	80

Figure 3. RMT-150C rock mechanics test system.

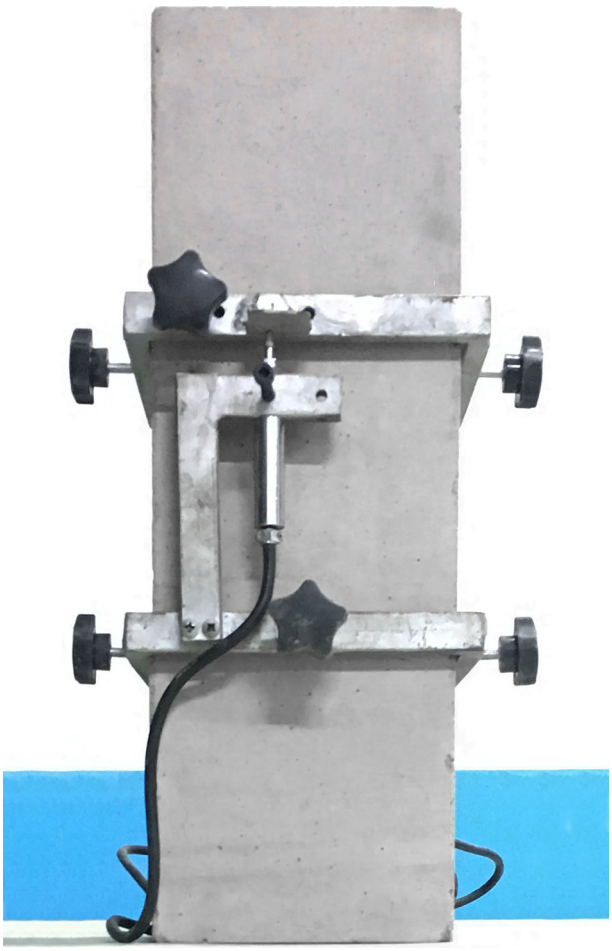

Figure 4. Displacement test device.

RESULTS AND DISCUSSION

Failure modes

The uniaxial compressive failure process of the prismatic specimen is showed in Figure 5. In this study, the failure processes of NAC, RAC and CRAC were roughly similar. In the initial loading stage, there was no crack on the surfaces of the specimen. After the peak load, many short fine cracks parallel to the loading direction appeared on the sides of the specimen. With the load further increasing, an oblique crack was formed between the short fine cracks. Afterwards, the oblique crack continued to expand and penetrated the whole side of the specimen. Finally, the residual load decreased slowly, which was provided by the friction force and residual bonding force on the fracture surface of the specimen.

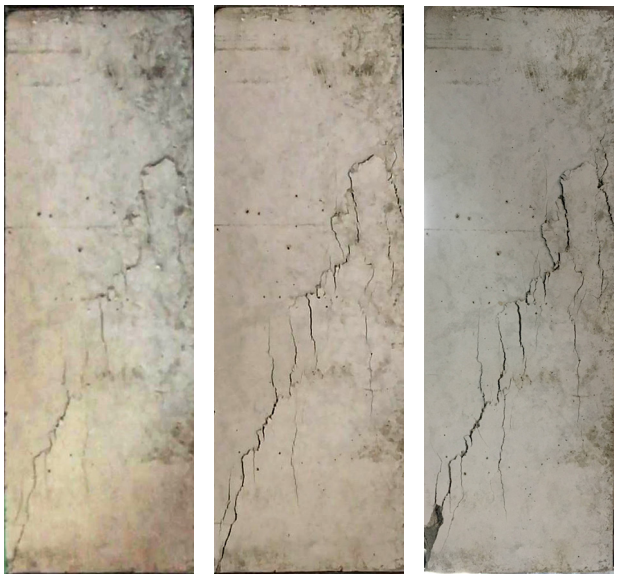

a) b) c)

Figure 5. The uniaxial compressive failure process: a) 0.9 fc in descending branch; b) 0.7 fc in descending branch; c) 0.5 fc in descending branch.

The uniaxial compressive failure modes of prismatic specimens are showed in Figure 6. The results showed that the failure modes of all specimens were shear failure, and the shear planes were perpendicular to the sides of the specimen. Moreover, the failure angles of NAC formed by oblique cracks and horizontal lines were in the range of 58°-64°, while those of RAC and CRAC were larger those that of NAC, about 63° – 75°. These results were consistent with the results reported by Xiao [7] and Gao [16].

Furthermore, by carefully observing the fracture surfaces of the specimens, it was found that NAC was mostly fractured along ITZ-1 and NM, but NA was rarely fractured. By contrast, RAC and CRAC were also fractured along ITZ-2 and OM, besides ITZ-1, ITZ-3, and NM.

Figure 6. The uniaxial compressive failure modes: a) NAC, θ = 61.10°; b) RAC-1, θ = 65.40°; c) RAC-2, θ = 69.10°; d) RAC-3, θ = 72.20°; e) CRAC-1, θ = 63.30°; f) CRAC-2, θ = 71.70°; g) CRAC-3, θ = 74.60°.

Stress-strain curves

The stress-strain curves of RAC and CRAC are showed in Figure 7. It can be seen that the change trends of stress-strain curves of RAC and CRAC were similar to that of NAC, which were composed of linear part of the ascending branch, nonlinear part of the ascending branch, and nonlinear part of the descending branch. More specifically, the stress-strain curve obeyed Hooke's law in the range of about 0.4 times of the peak stress, then its slope decreased gradually until reaching the peak stress. Finally, the stress decreased gradually with the increase of strain.

As can be seen from Figure 7a, as the substitution ratio of RCA increasing, the stress-strain curve of RAC gradually flattened, which meant that the material brittleness of RAC decreased. Hence, for NAC and RAC with similar peak stresses, such as NAC and RAC-1 in Figure 7a, the peak strain and ultimate strain of RAC increased. These findings were consistent with the results reported by Belén [8] and Tang [9]. It can be explained that compared with NAC with only one ITZ-1, the existence of ITZ-1, ITZ-2, and ITZ-3 in RAC can introduce more cracks generated and increase its strain, because ITZ is the weakest phase and the initial position for the generation of cracks in RAC [15].

As can be seen from Figure 7b, compared with RAC, CRAC showed the similar stress-strain curve, but its peak stress increased. It can be explained that CRCA improves the properties of ITZ-2 and ITZ-3 to a certain extent, but the essence that three types of ITZ exist in CRAC has not changed.

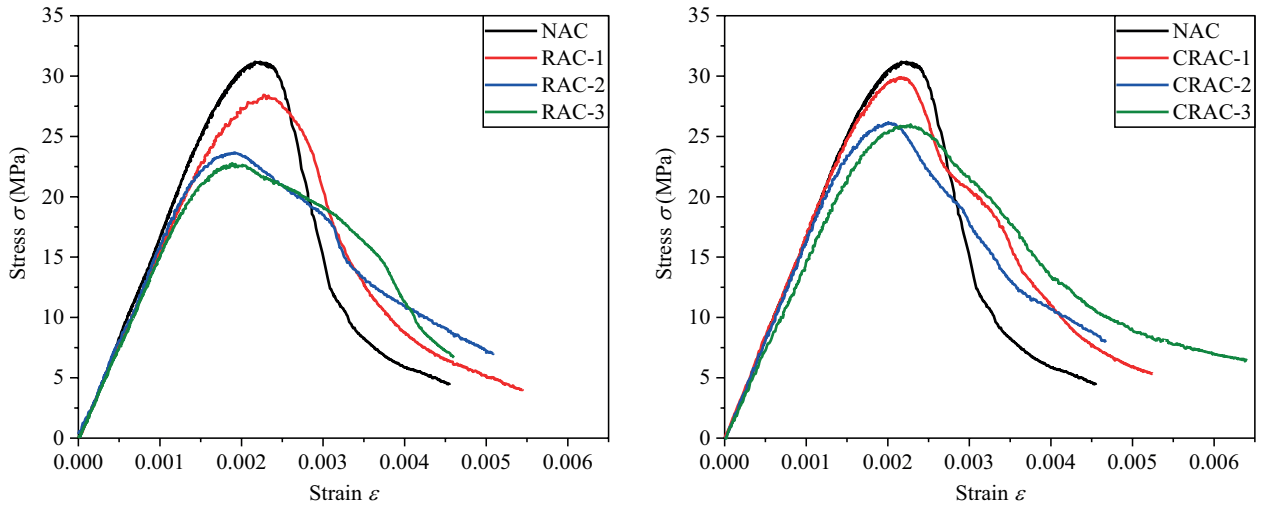

a) RAC b) CRAC

Figure 7. The stress-strain curves of RAC and CRAC: a) RAC; b) CRAC.

Peak stresses

The peak stresses of RAC and CRAC are showed in Table 4. It can be seen that as the substitution ratios of RCA and CRCA increasing, the peak stresses of RAC and CRAC gradually decreased, but those of CRAC were always higher than those of RAC. These phenomena were similar to the results reported by Luo [11]. Moreover, the percentage changes in peak stresses of RAC and CRAC are showed in Figure 8. Compared with NAC, when the substitution ratios of RCA and CRCA were 30 %, 70 %, and 100 % respectively, the peak stress of RCA decreased by 8.82 %, 24.14 %, and 26.96 % respectively, and the peak stress of CRCA decreased by 4.14 %, 16.06 %, and 16.64 % respectively. In addition, compared with RCA, the peak stress of CRCA increased by 5.13 %, 10.65 %, and 14.14 % respectively.

The above-mentioned phenomena can be explained as follows: as the substitution ratio of RCA increasing, the quantity of ITZ-1 in RAC decreases, while the quantity of ITZ-2 and ITZ-3 increase. The research found that the mechanical properties of RAC depend on the properties of ITZ-2 and ITZ-3 [17]. Therefore, the peak stress of RAC gradually decreases. However, after RCA is processed by accelerated carbonation, the properties of ITZ-2 in CRCA are improved. On the other hand, calcite promotes calcium silicate hydrate to nucleate and grow [13], and monocarbonate can also be generated in ITZ-3 by the reaction between calcite and aluminate, thus improving the properties of ITZ-3 [14]. Consequently, the peak stress of CRAC is higher than that of RCA.

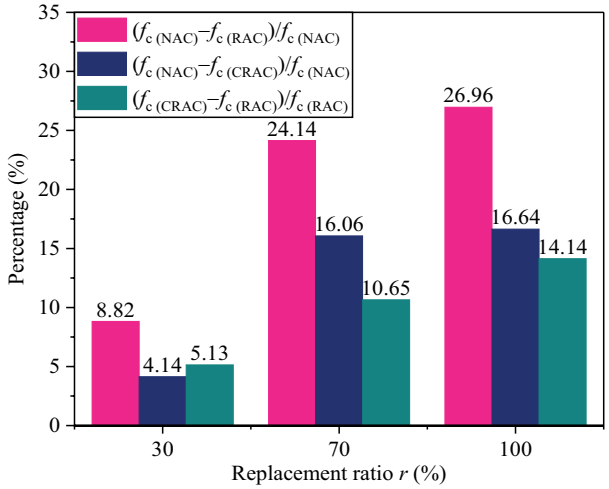

Figure 8. The percentage changes in peak stresses of RAC and CRAC.

In addition, the relationship between prismatic compressive strength and cubic compressive strength of RAC and CRAC is showed in Figure 9. Based on the test data in this study, $f_c' = 0.75\,f_{cu}$, $R^2 = 0.9996$ was obtained by linear regression, and it was roughly consistent with the provision of NAC in standard GB 50010-2010, $f_c^0 = 0.76\,f_{cu}$, which indicated that the relationship between the mechanical properties of RAC and CRAC was similar to that of NAC.

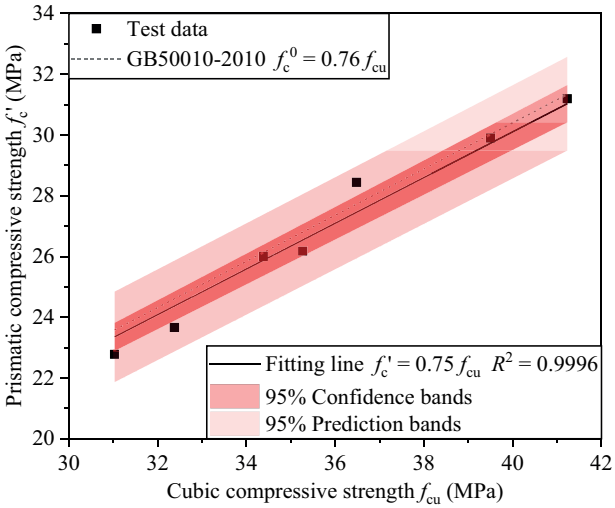

Figure 9. The relationship between prismatic compressive strength and cubic compressive strength.

Elastic moduli

Based on standard GB/T 50081-2019, the test values of elastic moduli corresponded to the secant slopes between 0.5 MPa and 1/3 f_c in the stress-strain curves, as showed in Table 4. In addition, based on standard GB 50010-2010, the calculated values of elastic moduli were obtained by Equation 1. Therefore, the relationship between the prediction values and test values of elastic moduli was obtained, as showed in Figure 10. Finally, the prediction model of elastic modulus was obtained by conducting linear regression on the test data in Figure 10, as showed in Equation 2.

Table 4. The indexes of stress-strain behaviour of RAC and CRAC.

Specimen type	f_{cu} (MPa)	f_c (MPa)	f_{cu}/f_c	E_c (GPa)	ε_c (10^{-6})	ε_u (10^{-6})
NAC	41.23	31.19	0.76	16.99	2166	2992
RAC-1	36.48	28.44	0.78	15.54	2270	3367
RAC-2	32.38	23.66	0.73	15.81	1916	3780
RAC-3	31.03	22.78	0.73	15.20	1885	3988
CRAC-1	39.50	29.90	0.76	16.99	2156	3571
CRAC-2	35.27	26.18	0.74	16.43	2005	3499
CRAC-3	34.38	26.00	0.76	14.82	2280	4055

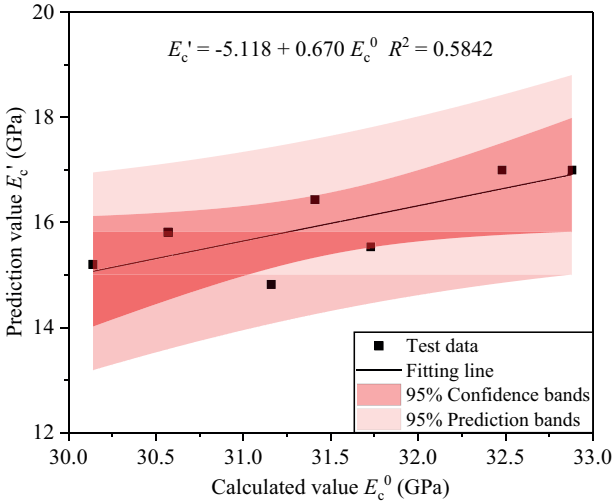

Figure 10. The relationship between the prediction values and test values of elastic moduli.

As showed in Figure 11, the prediction values obtained by Equation 2 were roughly consistent with the test values, which indicated that the prediction model had certain applicability. In addition, as the substitution ratios of RCA and CRCA increasing, the elastic moduli of RAC and CRAC gradually decreased, but those of CRAC were always higher than those of RAC. The reasons have been explained in the Sections "Stress-strain curves" and "Peak stresses"

$$E_c^0 = 10^2/(2.2 + 34.7/f_{cu})\ \text{(GPa)} \quad (1)$$

$$E_c' = -5.118 + 67/(2.2 + 34.7/f_{cu})\ \text{(GPa)} \quad (2)$$

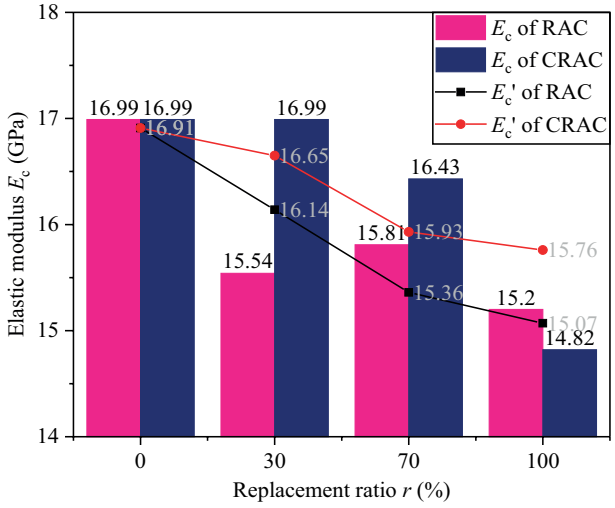

Figure 11. The elastic moduli of RAC and CRAC.

Peak strains

Based on standard GB 50010-2010, the calculated values of peak strains were obtained by Equation 3. Besides, the test values of peak strains are showed in Table 4. Therefore, the relationship between the prediction values and test values of peak strains was obtained, as showed in Figure 12. Finally, the prediction model of peak strain was obtained by conducting linear regression on the test data in Figure 12, as showed in Equation 4.

$$\varepsilon_c^0 = 700 + 172\sqrt{f_c}\ (10^{-6}) \quad (3)$$

$$\varepsilon_c' = 156 + 375\sqrt{f_c}\ (10^{-6}) \quad (4)$$

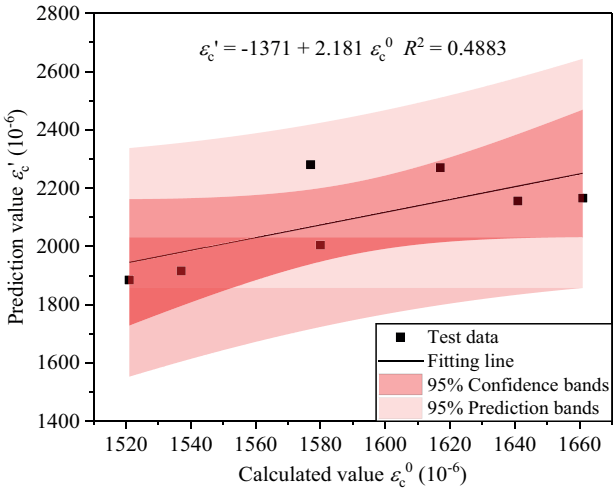

Figure 12. The relationship between the prediction values and test values of peak strains.

As showed in Figure 13, the prediction values obtained by Equation 4 were roughly consistent with the test values, which indicated that the prediction model had certain applicability. In addition, as the substitution ratios of RCA and CRCA increasing, the peak strains of RAC and CRAC gradually decreased, but those of CRAC were always higher than those of RAC. Tang [9] and Chen [18] also found that RCA reduced the peak strain of RAC, because as the substitution ratio of RCA increasing, the peak stress of RAC decreased obviously, while the elastic modulus of RAC changed little. However, for similar peak stresses, such as CRAC-2

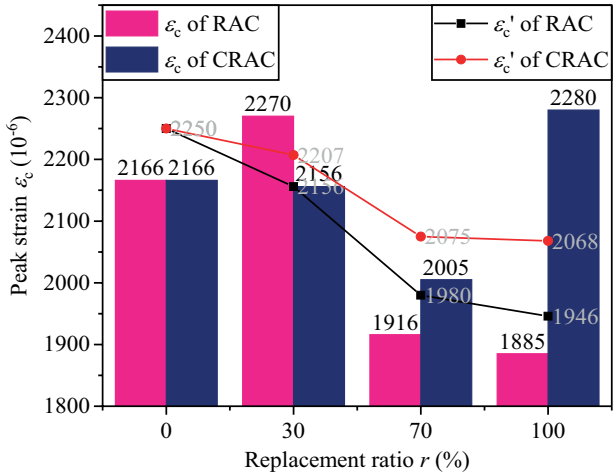

Figure 13. The peak strains of RAC and CRAC.

and CRAC-3 in Figure 7b, the peak strain of CRAC increased as the substitution ratio of CRCA increasing, this phenomenon was also reported by Belén [8].

Ultimate strains

Based on standard GB 50010-2010, the test values of ultimate strains corresponded to 0.5 f_c in the descending branches of the stress-strain curves, as showed in Table 4. In addition, the calculated values of ultimate strains were obtained by Equation 5. Therefore, the relationship between the prediction values and test values of ultimate strains was obtained, as showed in Figure 14. Finally, the prediction model of ultimate strains was obtained by conducting linear regression on the test data in Figure 14, as showed in Equation 6.

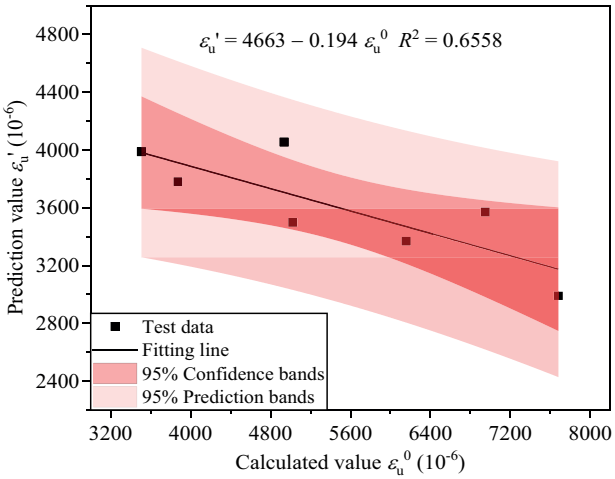

Figure 14. The relationship between the prediction values and test values of ultimate strains.

As showed in Figure 15, the prediction values obtained by Equation 6 were roughly consistent with the test values, which indicated that the prediction model had certain applicability. In addition, as the substitution ratios of RCA and CRCA increasing, the ultimate strains of RAC and CRAC gradually increased, but those of CRAC were always lower than those of RAC. The reasons have been explained in the Sections "Stress-strain curves" and "Peak stresses".

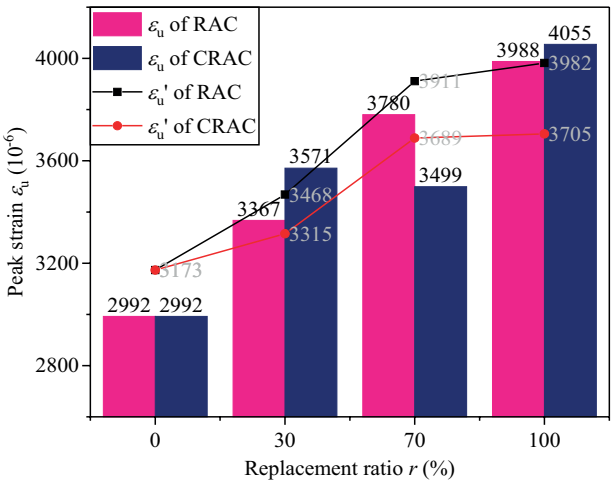

Figure 15. The ultimate strains of RAC and CRAC.

$$\varepsilon_c^0 = \varepsilon_c^0 \times (1 + 2b + \sqrt{1 + 4b})/2b \ \ (10^{-6}) \tag{5}$$

where $b = 0.157\, f_c^{0.785} - 0.905$

$$\varepsilon_u' = 4663 - 0.194[\varepsilon_c^0 \times (1 + 2b + \sqrt{1 + 4b})/2b] \tag{6}$$

where $b = 0.157\, f_c^{0.785} - 0.905$

Stress-strain constitutive models

At present, the stress-strain constitutive models of concrete are different in various standards. For example, the provisions in standard GB 50010-2002 are showed in Equations 7 and 8,

$$y = \begin{cases} ax + (3-2a)x^2 + (a-2)x^3 & x \le 1 \\ x/[b(x-1)^2 + x] & x > 1 \end{cases} \tag{7}$$

$$\begin{aligned} m &= E_c \varepsilon_c / (E_c \varepsilon_c - f_c) \\ b &= 0.157\, f_c^{0.785} - 0.905 \end{aligned} \tag{8}$$

the provisions in standard GB 50010-2010 are showed in Equations 9 and 10,

$$y = \begin{cases} mx/(m-1+x^m) & x \le 1 \\ x/[b(x-1)^2 + x] & x > 1 \end{cases} \tag{9}$$

$$\begin{aligned} m &= E_c \varepsilon_c / (E_c \varepsilon_c - f_c) \\ b &= 0.157\, f_c^{0.785} - 0.905 \end{aligned} \tag{10}$$

and the provisions in *fib* Model Code for Concrete Structures 2010 are showed in Equations 11 and 12,

$$y = (kx - x^2) / [1 + (k-2)x] \tag{11}$$

$$k = 19400 \times (0.1 f_c)^{1/3} / E_{c1} \tag{12}$$

where $x = \varepsilon/\varepsilon_c$, $y = \sigma/f_c$. Moreover, a and m are the calculated values of coefficients in ascending branches of constitutive models. The smaller the a is or the larger the m is, the smaller the proportion of plastic part in ascending branch is, and the greater the material brittleness is. Furthermore, b is the calculated value of coefficient in descending branch of the constitutive model. The larger the b is, the steeper the slope of descending branch is and the greater the material brittleness is. Besides, k is the calculated value of coefficient of the constitutive model. The larger the k is, the larger the proportion of plastic part in ascending branch is, the gentler the slope of descending branch is, and the smaller the material brittleness is. E_{c1} is the secant modulus between original point and peak stress.

Based on Equations 8, 10, and 12, the coefficients of stress-strain curves of RAC and CRAC are obtained, as showed in Table 5. It can be seen that as the substitution

ratios of RCA and CRCA increasing, a and k gradually increased, while m and b gradually decreased, which indicated that the material brittleness of RAC and CRAC gradually decreased. These results were consistent with the stress-strain curves of RAC and CRAC in Figure 16.

As showed in Figure 17, the stress-strain calculated curves obtained by Table 5 and the stress-strain test curves were compared. It can be seen that in terms of the ascending branches, the calculated curves of a and k almost coincided, but they deviated far from the test curves. By contrast, the calculated curves of m almost coincided with the test curves. With respect to the descending branches, the change trends of calculated curves of k differed from those of test curves, while those

Table 5. The indexes of stress-strain behaviour of RAC and CRAC.

Specimen type	f_c (MPa)	ε_c (10^{-6})	E_c (GPa)	E_{c1} (GPa)	a	b	m	k
NAC	31.19	2166	16.99	14.40	2.01	1.43	6.56	1.97
RAC-1	28.44	2270	15.54	12.53	2.04	1.27	5.16	2.19
RAC-2	23.66	1916	15.81	12.35	2.10	0.98	4.57	2.09
RAC-3	22.78	1885	15.20	12.08	2.12	0.92	4.88	2.11
CRAC-1	29.90	2156	16.99	13.87	2.03	1.36	5.44	2.02
CRAC-2	26.18	2005	16.43	13.06	2.07	1.13	4.87	2.05
CRAC-3	26.00	2280	14.82	11.40	2.08	1.12	4.34	2.34

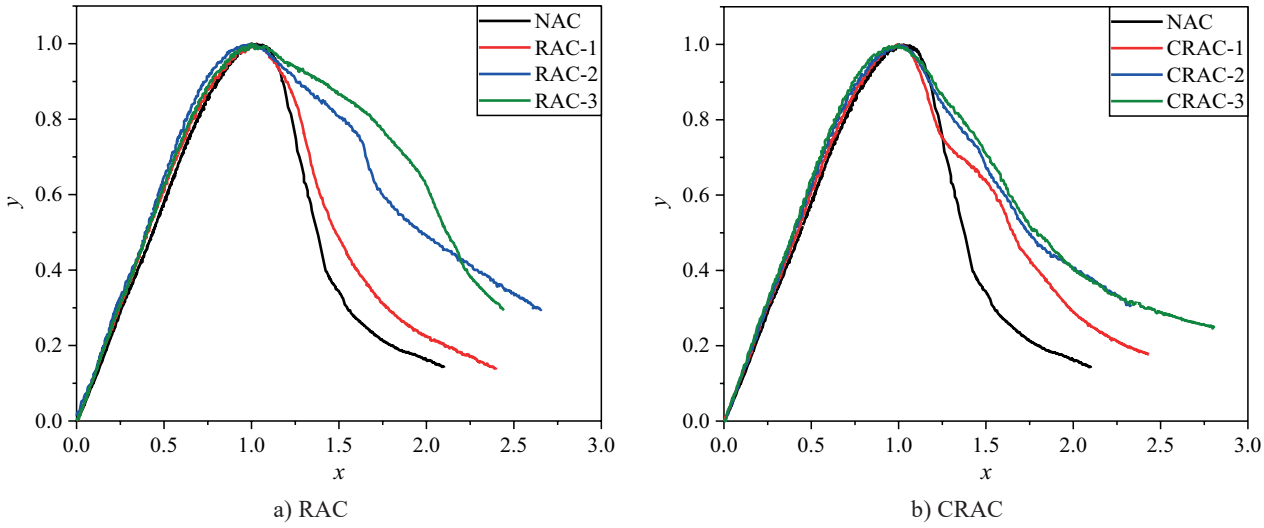

a) RAC b) CRAC

Figure 16. The stress-strain curves of RAC and CRAC: a) RAC; b) CRAC.

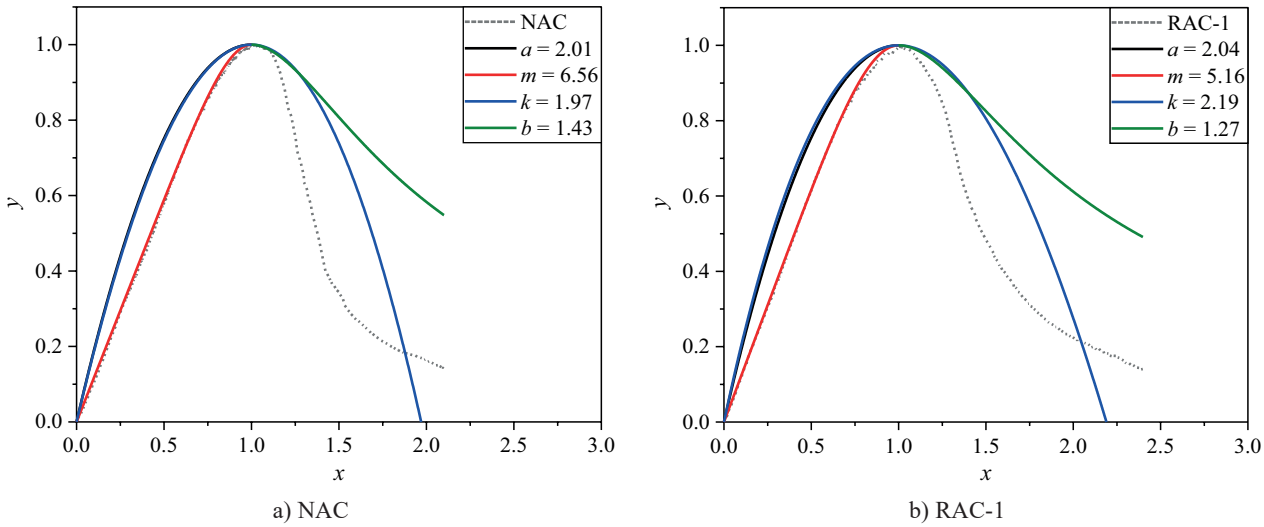

a) NAC b) RAC-1

Figure 17. The stress-strain calculated curves and the stress-strain test curves: a) NAC; b) RAC-1. *(Continue on next page)*

of b were in good agreement with those of test curves. Therefore, Equations 9 and 10, which were specified in standard GB 50010-2010, have the best applicability to RAC and CRAC in this study.

Through fitting the stress-strain test curves of RAC and CRAC by Equation 9, the stress-strain fitting curves as well as m' and b' were obtained, as showed in Figure 18. Therefore, the relationships between calculated values and prediction values of coefficients were obtained, as showed in Figure 19. Next, Equation 14 was obtained by fitting the test data in Figure 19 using linear regression. Finally, as showed in Equations 13 and 14, the stress-strain constitutive model suitable for RAC and CRAC in this study was obtained. As showed in Figure 20, the stress-strain prediction curves based on Equations 13 and 14 were compared with the stress-strain test curves. It can be seen that the prediction curves nearly coincided with the test curves, which indicated that the proposed constitutive model had good applicability to the test data.

$$y = \begin{cases} m'x/(m'-1+x^{m'}) & x \le 1 \\ x/[b'(x-1)^2+x] & x > 1 \end{cases} \quad (13)$$

$$m' = 1.438 \times (E_c\varepsilon_c/(E_c\varepsilon_c - f_c) - 2.068$$
$$b' = 2.199 f_c^{0.785} - 24.789 \quad (14)$$

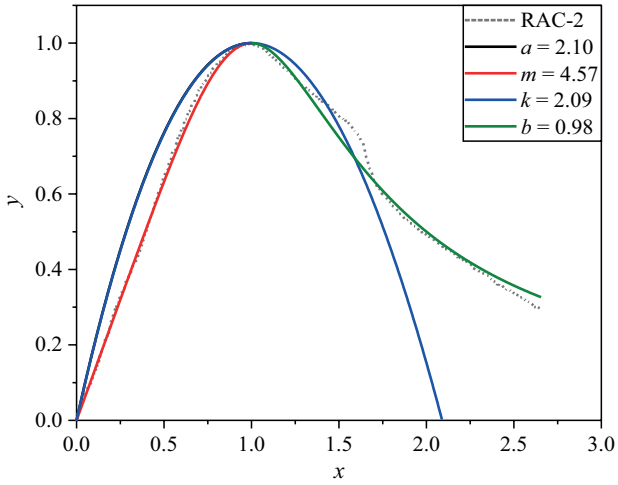

c) RAC-2

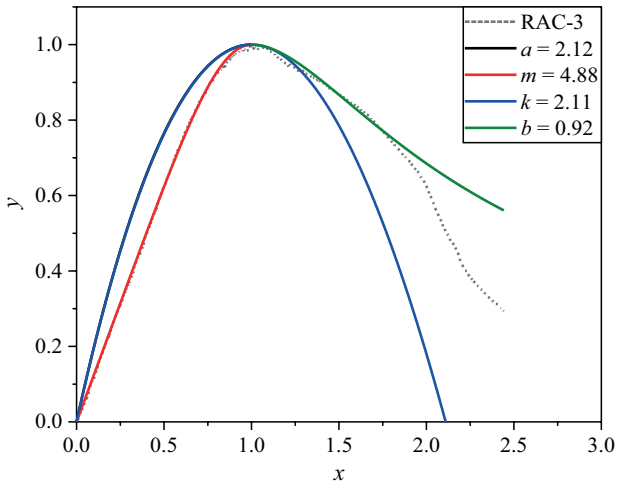

d) RAC-3

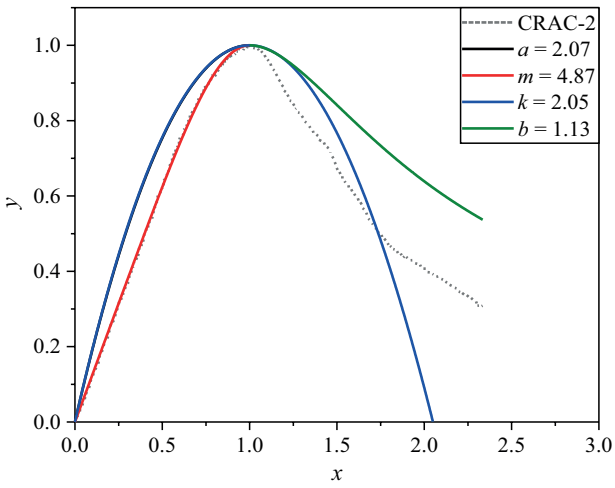

f) CRAC-2

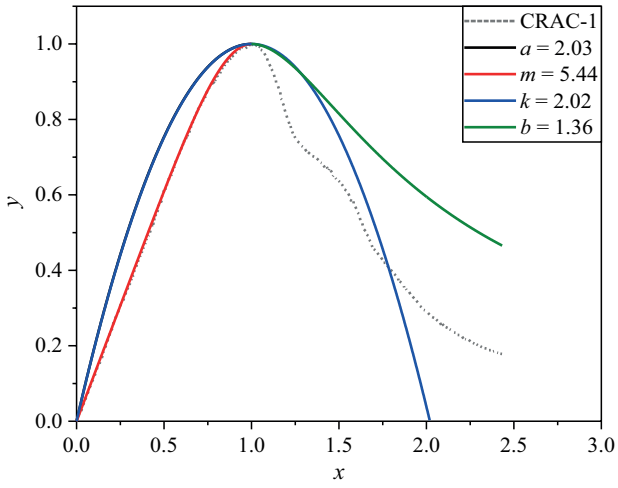

e) CRAC-1

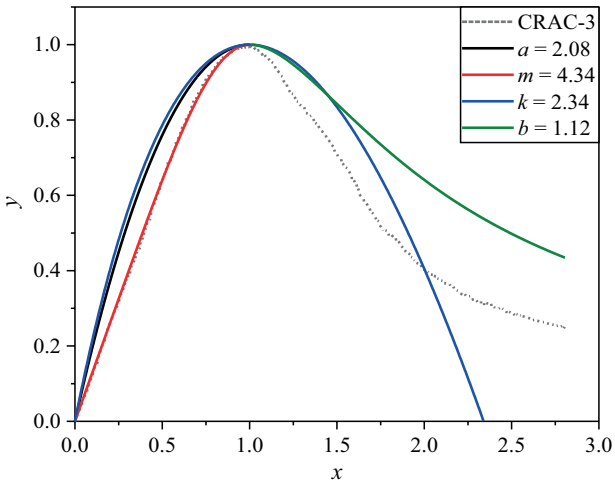

g) CRAC-3

Figure 17. TThe stress-strain calculated curves and the stress-strain test curves: c) RAC-2; d) RAC-3; e) CRAC-1; f) CRAC-2; g) CRAC-3.

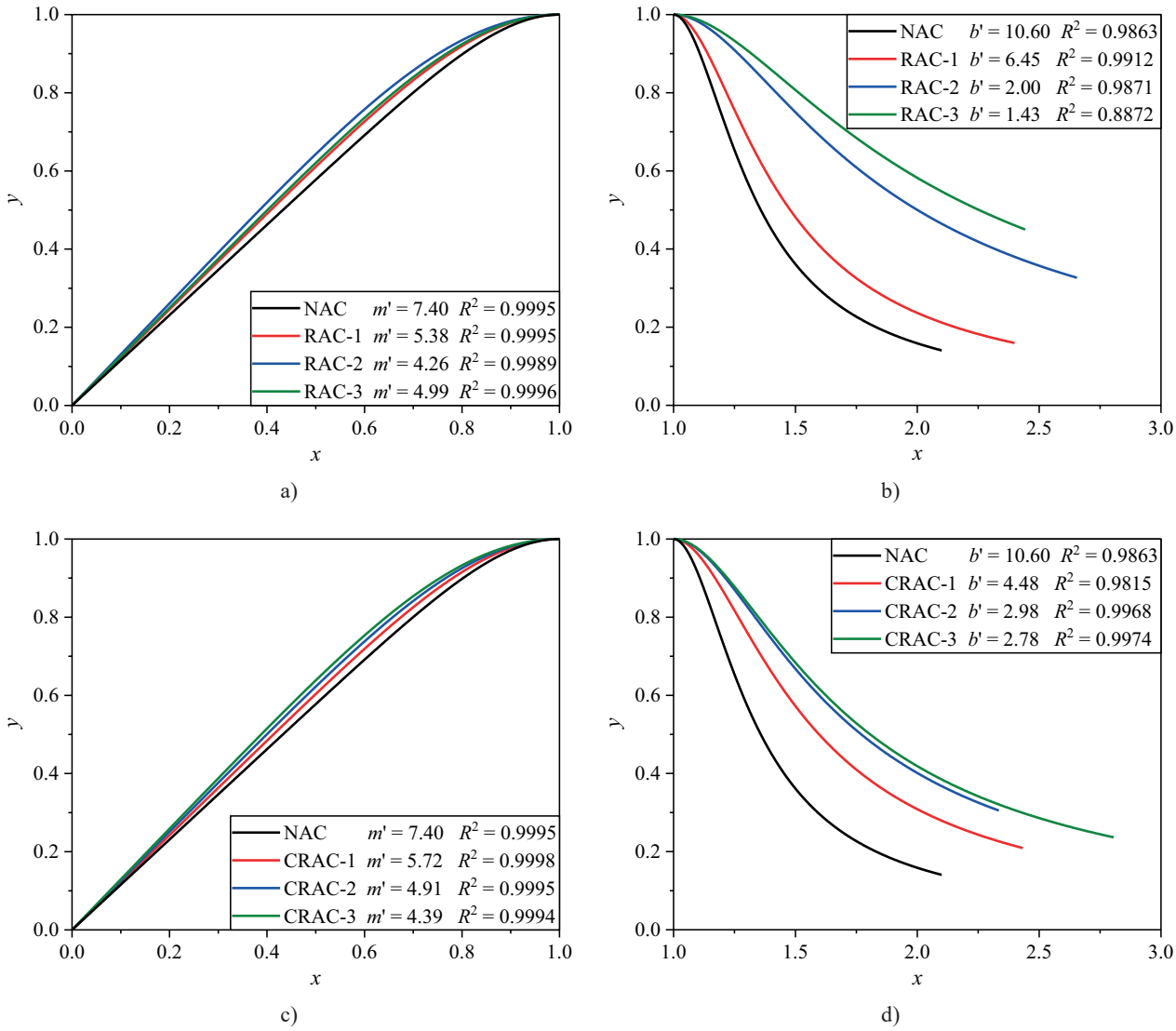

Figure 18. The stress-strain fitting curves: a) ascending branches of RAC; b) descending branches of RAC; c) ascending branches of CRAC; d) descending branches of CRAC.

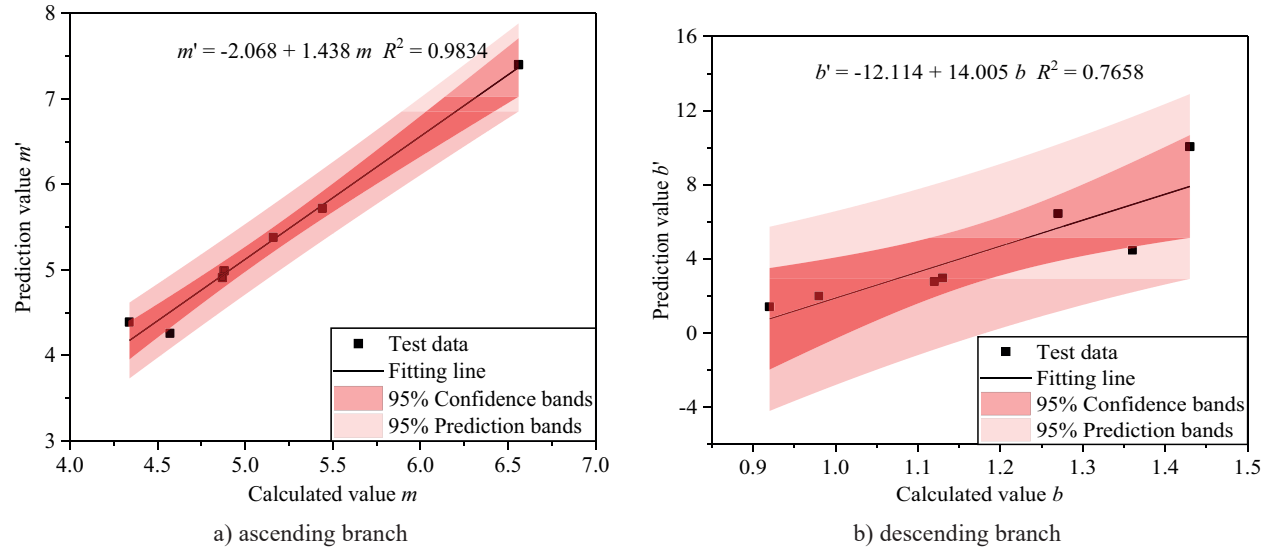

Figure 19. The relationships between calculated values and prediction values of coefficients: a) ascending branch; b) descending branch.

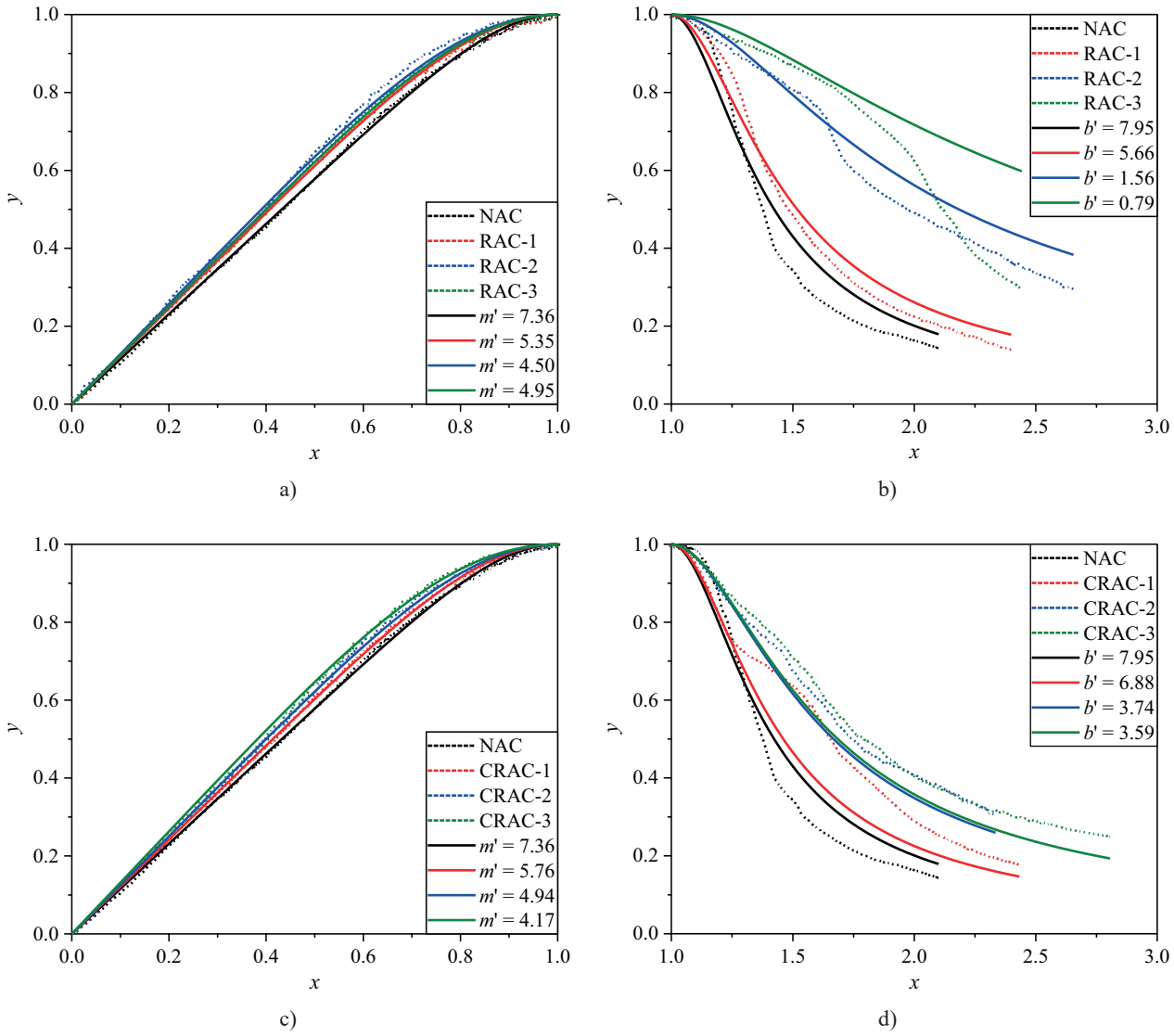

Figure 20. The stress-strain prediction curves and the stress-strain test curves: a) ascending branches of RAC; b) descending branches of RAC; c) ascending branches of CRAC; d) descending branches of CRAC.

CONCLUSIONS

The influences of RCA and CRCA with different substitution ratios on the stress-strain behaviour of RCA and CRCA were studied, and the main conclusions are as follows:

- The failure modes of all specimens were shear failure, but the failure angles of RAC and CRAC were larger than those of NAC, which were in the range of 63°–75° and 58°–64° respectively.
- As the substitution ratio of RCA increasing, the stress-strain curve of RAC gradually flattened, which meant its brittleness decreased. Moreover, its peak stress, elastic modulus, and peak strain decreased continuously, while its ultimate strain increased continuously. Compared with RAC, CRAC showed the similar stress-strain curve, but its brittleness was slightly higher. Furthermore, its peak stress, elastic modulus, and peak strain increased, while its ultimate strain decreased.
- Based on linear regression analysis and relevant standards, the prediction models of peak stress, elastic modulus, peak strain, and ultimate strain, as well as the stress-strain constitutive models of RAC and CRAC were proposed, which had a good applicability to the test data.
- The stress-strain behaviour of CRAC were similar to that of RAC, and the differences between them were attributed to the fact that accelerated carbonation improved the quality of CRCA, thus improving the mechanical properties of CRAC.

Notation

f_c prismatic compressive strength or peak stress

f_{cu} cubic compressive strength

E_c test value of secant modulus between 0.5 MPa and 1/3 f_c

E_c^0 calculated value of secant modulus between 0.5 MPa and 1/3 f_c

E_c' prediction value of secant modulus between 0.5 MPa and 1/3 f_c

E_{c1} secant modulus between original point and peak stress

σ stress

ε strain

ε_c test value of peak strain

ε_c^0 calculated value of peak strain

ε_c' prediction value of peak strain

ε_u test value of ultimate strain corresponding to 0.5 f_c in descending branch

ε_u^0 calculated value of ultimate strain corresponding to 0.5 f_c in descending branch

ε_u' prediction value of ultimate strain corresponding to 0.5 f_c in descending branch

θ uniaxial compressive failure angle of prismatic specimen

x $x = \varepsilon/\varepsilon_c$, normalized strain

y $y = \sigma/f_c$, normalized stress

a calculated value of coefficient in ascending branch of constitutive model

m calculated value of coefficient in ascending branch of constitutive model

m' prediction value of coefficient in ascending branch of constitutive model

b calculated value of coefficient in descending branch of constitutive model

b' prediction value of coefficient in descending branch of constitutive model

k calculated value of coefficient in constitutive model

Acknowledgments

This work was supported by Joint Funds of the National Natural Science Foundation of China (Grant No. U1904188), and the Key Science and Technology Program of Henan Province, China (Grant No. 202102310253).

REFERENCES

1. Zhang Y.R., Luo W., Wang J.J., Wang Y.F., Xu Y.Q., Xiao J.Z. (2019): A review of life cycle assessment of recycled aggregate concrete. *Construction and Building Materials*, *209*, 115-125. doi: 10.1016/j.conbuildmat.2019.03.078
2. Ding Y.H., Wu J., Xu P., Zhang X.G., Fan Y.H. (2021): Treatment methods for the quality improvement of recycled concrete aggregate (RCA) - A review, *Journal of Wuhan University of Technology-Mater. Sci. Ed.*, *36* (1), 77-92. doi: 10.1007/s11595-021-2380-3
3. Mistria A., Bhattacharyyaa S.K., Dhami N., Mukherjee A., Barai S.V. (2020): A review on different treatment methods for enhancing the properties of recycled aggregates for sustainable construction materials. *Construction and Building Materials*, *233*, 117894. doi: 10.1016/j.conbuildmat.2019.117894
4. Wang B., Yan L.B., Fu Q.N., Kasal B. (2021): A Comprehensive Review on Recycled Aggregate and Recycled Aggregate Concrete. *Resources, Conservation & Recycling*, *171*, 105565. doi: 10.1016/j.resconrec.2021.105565
5. Wang J.G., Zhang J.X., Cao D.D., Dang H.X., Ding B. (2020): Comparison of recycled aggregate treatment methods on the performance for recycled concrete. *Construction and Building Materials*, *234,* 117366. doi: 10.1016/j.conbuildmat.2019.117366
6. Pu Y.H., Li L., Wang Q.Y., Shi X.S., Fu L., Zhang G.M., Luan C.C., Abomohra A. E. (2021): Accelerated carbonation treatment of recycled concrete aggregates using flue gas: A comparative study towards performance improvement. *Journal of CO2 Utilization*, *43*,101362. doi: 10.1016/j.jcou.2020.101362
7. Xiao J.Z., Li J.B., Zhang C. (2005): Mechanical properties of recycled aggregate concrete under uniaxial loading. *Cement and Concrete Research*, *35* (6), 1187-1194. doi: 10.1016/j.cemconres.2004.09.020
8. Belén G.F., Fernando M.A., Diego C.L., Sindy S.P. (2011): Stress-strain relationship in axial compression for concrete using recycled saturated coarse aggregate. *Construction and Building Materials*, *25* (5), 2335-2342. doi: 10.1016/j.conbuildmat.2010.11.031
9. Tang Z., Hu Y., Tam V.W.Y., Li W.G. (2019): Uniaxial compressive behaviors of fly ash/slag-based geopolymeric concrete with recycled aggregates. *Cement and Concrete Composites*, *104,* 103375. doi: 10.1016/j.cemconcomp.2019.103375
10. Li L., Poon C.S., Xiao J.Z., Xuan D.X. (2017): Effect of carbonated recycled coarse aggregate on the dynamic compressive behavior of recycled aggregate concrete. *Construction and Building Materials*, *151*, 52-62. doi: 10.1016/j.conbuildmat.2017.06.043
11. Luo S.R., Ye S.C., Xiao J.Z., Zheng J.L., Zhu Y.T. (2018): Carbonated recycled coarse aggregate and uniaxial compressive stress-strain relation of recycled aggregate concrete. *Construction and Building Materials*, *188*, 956-965. doi: 10.1016/j.conbuildmat.2018.08.159
12. Fang X.L., Zhan B.J., Poon C.S. (2021): Enhancement of recycled aggregates and concrete by combined treatment of spraying Ca^{2+} rich wastewater and flow-through carbonation. *Construction and Building Materials*, *277*, 122202. doi: 10.1016/j.conbuildmat.2020.122202
13. Ouyang X.W., Wang L.Q., Xu S.D., Ma Y.W., Ye G. (2020): Surface characterization of carbonated recycled concrete fines and its effect on the rheology, hydration and strength development of cement paste. *Cement and Concrete Composites*, *114*, 103809. doi: 10.1016/j.cemconcomp.2020.103809
14. Zhan B.J., Xuan D.X., Poon C.S., Scrivener K.L. (2020): Characterization of interfacial transition zone in concrete

prepared with carbonated modeled recycled concrete aggregates. *Cement and Concrete Research*, *136*, 106175. doi: 10.1016/j.cemconres.2020.106175

15. Xiao J.Z., Li W.G., Corr D.J., Shah S.P. (2013): Effects of interfacial transition zones on the stress-strain behavior of modeled recycled aggregate concrete. *Cement and Concrete Research*, *52*, 82-99. doi: 10.1016/j.cemconres.2013.05.004
16. Gao D.Y., Zhang L.J., Nokken M. (2017): Compressive behavior of steel fiber reinforced recycled coarse aggregate concrete designed with equivalent cubic compressive strength. *Construction and Building Materials*, *141*, 235-244. doi: 10.1016/j.conbuildmat.2017.02.136
17. Yue G.B., Ma Z.M., Liu M, Liang C.F., Ba G.Z. (2020): Damage behavior of the multiple ITZs in recycled aggregate concrete subjected to aggressive ion environment. *Construction and Building Materials*, *245*, 118419. doi: 10.1016/j.conbuildmat.2020.118419
18. Chen A.J., Han X.Y., Chen M., Wang X.Y., Wang Z.H., Guo T.T. (2020): Mechanical and stress-strain behavior of basalt fiber reinforced rubberized recycled coarse aggregate concrete. *Construction and Building Materials*, *260*, 119888. doi: 10.1016/j.conbuildmat.2020.119888